RSC Advances

PAPER

View Article Online
View Journal | View Issue

Cite this: *RSC Adv.*, 2016, **6**, 5141

Synthesis of new phosphorescent imidoyl-indazol and phosphine mixed ligand Cu(I) complexes – structural characterization and photophysical properties†

Alan R. Cabrera,*[ae] Ivan A. Gonzalez,[a] Diego Cortés-Arriagada,[a] Mirco Natali,[b] Heinz Berke,[c] Constantin G. Daniliuc,[d] María B. Camarada,[e] Alejandro Toro-Labbé,[a] Rene S. Rojas[a] and Cristian O. Salas[a]

Four mononuclear Cu(I) complexes were prepared, described as $[Cu(N,N)_2]PF_6$ (**1**) and $[Cu(N,N)(P,P)]PF_6$ (**2–4**), where *N*,*N* is *N*-(1-(2*H*-indazol-2-yl)ethylidene)-2,6-diisopropylaniline and *P*,*P* are phosphine derived ancillary ligands (bis[2-(diphenylphosphino)phenyl]ether (POP), bis(diphenylphosphino)ethane (dppe) or 2 PPh_3). These new species were characterized by NMR, FT-IR, elemental analyses, cyclic voltammetry, UV-Vis – emission spectroscopy, transient absorption spectroscopy and DFT calculations. In addition, complexes **1** and **2** were characterized by X-ray diffraction. The four complexes showed an MLCT absorption band between 400 and 450 nm, in addition to a weakly structured phosphorescence in a 4 : 1 ethanol : methanol glassy matrix at 77 K. Complexes **2–4** have emission profiles that resemble the phosphorescence of the protonated *N*,*N* ligand, suggesting a triplet LC character of the lowest lying excited state at 77 K. By contrast, a mixed MLCT/LC triplet emission is most likely responsible for the phosphorescence in complex **1**. Weak ligand-centered emission is also detected in the solid state at room temperature but only in the case of complexes **2** and **4**, suggesting thermally activated deactivation processes in the case of **1** and **3**. Notably, the transient absorption spectroscopy of complexes **2–4** in CH_2Cl_2 solution confirms a strong contribution from a ligand-centered (LC) triplet excited state, pointing towards a mixed ^{3}MLCT/^{3}LC character of the transient species in solution at room temperature, undergoing a non-radiative deactivation in the μs time-scale. This behavior markedly differs from that observed for complex **1**, whose short-lived ^{3}MLCT excited state is followed by ultrafast transient absorption spectroscopy.

Received 2nd October 2015
Accepted 23rd December 2015

DOI: 10.1039/c5ra20450j

www.rsc.org/advances

Introduction

In recent years research on the development of optoelectronic devices has been intensified, mainly triggered by the enormous technological advances in areas such as flat displays and energy-efficient lighting.[1] Transition metal complexes have played a leading role in the development of photochemical molecular devices, including nonlinear optics (NLO), organic light emitting diodes (OLED), and light emitting electrochemical cells (LEEC). All these systems require a specific and controlled response to an external energy input.[2] To date, the most widely used devices are those based on second or third row transition metals, such as Ru, Re, Ir, Pt, and Os. However, these metals are of high cost and low natural abundance, generating an expensive large scale production costs of the emitting devices.[3] One potential and viable solution is to use cheaper first-row transition metals, which have greater abundance. In this respect, emitting devices based on Cu(I) have attracted great attention, as copper is a metal of low toxicity and has been successfully tested in OLEDs.[4]

The Cu(I) metal center has a $3d^{10}$ electronic configuration, and preferably form tetrahedral complexes. The work made by McMillin *et al.* established since the late 1970s the foundation of

[a]*Nucleus Millennium Chemical Processes and Catalysis, Faculty of Chemistry, Pontificia Universidad Católica de Chile, Casilla 306, Santiago-22, Chile. E-mail: arcabrer@uc.cl*

[b]*Department of Chemical and Pharmaceutical Sciences and Centro Interuniversitario per la Conversione Chimica dell'Energia Solare (sez. di Ferrara), University of Ferrara, Via Fossato di Mortara 17–19, 44121 Ferrara, Italy*

[c]*Chemisches Institut, Universität Zürich, Winterthurer Strasse 190, CH-8057 Zürich, Switzerland*

[d]*Organisch-Chemisches Institut, Universität Münster, Corrensstrasse 40, 48149 Münster, Germany*

[e]*Universidad Bernardo O Higgins, Departamento de Ciencias Químicas y Biológicas, Laboratorio de Bionanotecnología, General Gana 1702, Santiago, Chile*

† Electronic supplementary information (ESI) available: Including spectroscopic and crystallographic details (CIF). CCDC 1422058 for **1** and 1422059 for **2**. For ESI and crystallographic data in CIF or other electronic format see DOI: 10.1039/c5ra20450j

a chemistry with Cu(I) complexes bearing *N*,*N* phenanthroline ligands and their derivatives of the type $[Cu(N,N)_2]^+$. A basis was developed for the study of the relationship between molecular structure and photophysical properties of these complexes in solution.[5] The absorption spectra of these types of complexes show bands in the UV region corresponding to LC (ligand centered) transitions, while in the visible region the spectra exhibit bands corresponding to MLCT (metal-to-ligand charge transfer) transitions, which are significantly influenced by the nature of the coordinated ligands. Due to the presence of a d^{10} closed shell and thus to the absence of d–d electronic transitions, these complexes exhibit triplet MLCT emission.[6] The efficiency, however, is usually low in solution due to competitive non-radiative deactivations of the excited state accompanied by the structural reorganization of the complexes and/or the formation of exciplexes,[7] whereas in the solid state it is expected that higher emission yields can be achieved precluding formation of exciplexes or dimeric aggregates, mainly because of a completed coordination sphere by coordination of a solvent molecule to the copper center.[8] To overcome this issue the strategy adopted for $[Cu(N,N)_2]^+$ complexes was based on the use of highly sterically hindered *N*,*N* ligands which prevented (or at least minimized) the possibility of structural rearrangement and exciplex formation in the excited state.[6,8] However, even in this case the low emission energies were usually responsible for the unexceptional photoluminescence properties.

Other strategies were applied to further understand the issues experienced when studying the heteroleptic complexes of the type $[Cu(N,N)(P,P)]^+$, which contain bidentate phosphorus-based ligands replacing in the tetrahedral arranged homoleptic systems one *N*,*N* ligand.[9] The use of phosphine ligands, which have a greater electron-withdrawing character than phenanthrolines,[9l] stabilizes the HOMO of the Cu(I) complex. In this case, the LUMO is still localized in the *N*,*N* ligand, therefore the *P*,*P* one is the responsible for the modulation of the MLCT energy which could result in an important effect over the emission efficiencies (according to the energy-gap law).[6,9] On the other hand, the distinct coordination modes of different *P*,*P* ligands into the copper center may affect the energy of the MLCT emission resulting in color tunability *via* *P*,*P* substitution.[9,10] Indeed, the choice of the phosphine ligand is crucial for the optimization of the photophysical properties of the heteroleptic Cu(I) compounds, which are influenced by the P–Cu–P bond angles, the size of the cone angle of monodentate phosphines, and the bite angle of the bidentate phosphines.[10] Hence, the development of heteroleptic complexes proved to be an important and fundamental step forward in the aforementioned applications.

In this work four mononuclear Cu(I) complexes were synthesized and structurally characterized, one homoleptic of type $[Cu(N,N)_2]^+$, and three heteroleptic of type $[Cu(N,N)(P,P)]^+$ (*N*,*N* = *N*-(1-(2*H*-indazol-2-yl)ethylidene)-2,6-diisopropylaniline). The isopropyl substituent exerts great steric hindrance, preventing structural rearrangement, and the indazole ring system is mainly responsible for the electronic delocalization in the ligand, favoring a charge transfer necessary for optoelectronic devices such as NLO, DSSC, OLED and LEEC.[9,11] The *P*,*P* ligand systems are three different types of phosphines, namely bis[2-(diphenyl phosphino)phenyl]ether (POP), bis(diphenylphosphino)ethane (dppe) and triphenylphosphine (PPh_3).

Results and discussion

Synthesis and structural characterization

The copper(I) complexes with the *N*,*N* ligand (*N*-(1-(2*H*-indazol-2-yl)ethylidene)-2,6-diisopropylaniline) and the *P*,*P* ancillary phosphine ligands (*P*,*P* = POP, dppe and PPh_3) {$[Cu(N,N)_2]PF_6$ (**1**), $[Cu(N,N)(POP)]PF_6$ (**2**), $[Cu(N,N)(dppe)]PF_6$ (**3**) and $[Cu(N,N)(PPh_3)_2]PF_6$ (**4**)}, were prepared according to literature methods, applying a severe control of the reaction stoichiometries (see Scheme 1).[9a,12–14] The *N*,*N* ligand (*N*-(1-(2*H*-indazol-2-yl)ethylidene)-2,6-diisopropylaniline) was previously reported by our group.[15] The homoleptic complex **1** was obtained in a straightforward synthesis by addition of $[Cu(CH_3CN)_4]PF_6$ to a solution of 2 equivalents of the *N*,*N* ligand in acetonitrile. The heteroleptic species (**2–4**) were prepared in a two-step reaction *via* addition of one equivalent of the *N*,*N* ligand to a $[Cu(CH_3CN)_4]PF_6$ solution in acetonitrile, followed by the addition of another equivalent of the *phosphorus* ligands (Scheme 1) furnishing high yields. Complexes **1–4** were air and thermally stable in solution as well as in the solid state. They were fully characterized by NMR, IR, elemental analyses and for complexes **1** and **2** in addition by X-ray diffraction analyses.

Selected spectroscopic parameters of complexes **1–4** and of the *N*,*N* ligand are summarized in Table 1. The NMR spectra of the complexes are consistent with the formation of mononuclear pseudo-tetrahedral species coordinated by two bidentate ligands. In most cases, the ^1H and ^{13}C NMR spectra display low field shifts compared to the free *N*,*N* ligand due to the effect of coordination. The ^{31}P NMR spectra of compounds **2–4** exhibit singlets at −12.0, 7.4 and 1.3 ppm, respectively, suggesting that the *phosphorus* ligands are symmetrically bounded to the metal centers comparable to previously reported Cu(I) complexes of related types.[9d,10,16,17] In addition for the coordinated phosphine ligands, significant chemical shift changes are observed with respect to the free phosphine. The ^{19}F and ^{31}P NMR spectra of complexes **1–4** show similar chemical shifts for the PF_6^- counterion in CD_2Cl_2, indicating that these counterions are "free" ions and are not or to a very small extent only ion-pairing with the cationic complex parts (^{19}F: −72.8 ppm (d); ^{31}P: −144.3 ppm (sept)).

The molecular structures of the Cu(I) complexes **1** and **2** were determined by X-ray diffraction studies and are shown in Fig. 1 and 2, respectively. In complex **1**, the metal center has a distorted tetrahedral geometry as a consequence of the small bite angles of the two chelating *N*,*N* ligands [N3A–Cu1–N2A 79.1(2)°; N3B–Cu1–N2B 78.8(2)°] and a hindered substituent environment around the Cu(I) center, due to the isopropyl groups, which is corroborated by the dihedral angles [N1B–N2B–Cu1–N2A 112.1(3)°; N1B–N2B–Cu1–N3A −161.0(3)°]. On the other hand, complex **2** exhibits a less distorted tetrahedral geometry with a greater bite angle from the phosphine ligand [N2–Cu1–N3 77.0(2)°; P1–Cu1–P2 111.1(1)°]. The highly congested environment contributed by this ligand affects the Cu–N distances,

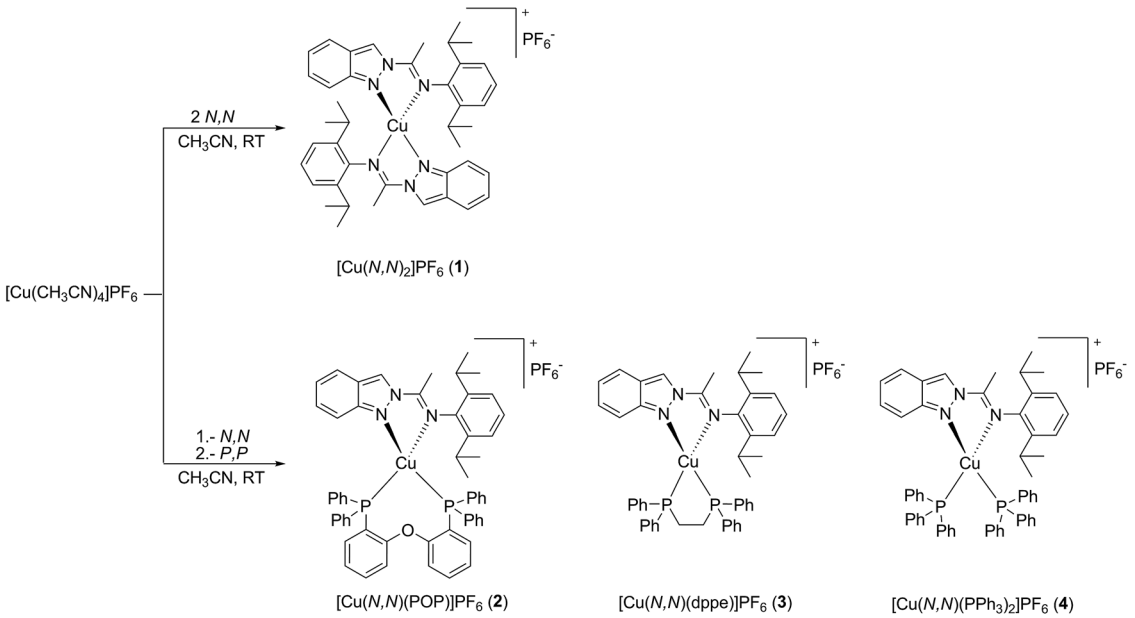

Scheme 1 Synthetic routes for complexes **1–4**.

Table 1 Selected NMR parameters of the Cu(I) complexes **1–4**[a]

	N,N	**1**	**2**	**3**	**4**
δ ^{1}H NMR (ppm)					
$\boldsymbol{H}^{C=N\ (indazole)}$	8.98	8.80	9.06	9.06	9.22
$\boldsymbol{H}C^{iPr}$	2.74	2.79	2.59	2.81	2.53
$C\boldsymbol{H}_3^{C=N}$	2.37	2.46	2.54	2.71	2.68
$C\boldsymbol{H}_3^{iPr}$		1.00	0.62	1.16	0.72
		0.34	0.49	0.80	0.37
δ ^{13}C{H}NMR (ppm)					
$^{Me}\boldsymbol{C}^{=N}$	154.7	157.4	157.3	160.3	158.0
$H\boldsymbol{C}^{iPr}$		28.8	28.9	29.4	29.1
$\boldsymbol{C}H_3^{iPr}$		23.5	24.6	23.7	24.5
		22.9	22.9	23.4	23.2
$\boldsymbol{C}H_3^{C=N}$	16.5	16.1	17.9	15.8	18.1
δ ^{31}P{H}NMR (ppm)					
$\boldsymbol{P}F_6^-$	—	−144.3	−144.3	−144.4	−144.3
P,P	—	—	−12.0	7.4	1.3

[a] In CD_2Cl_2 solution.

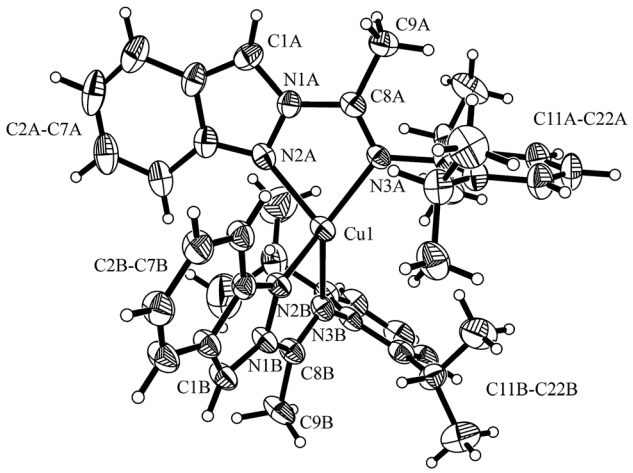

Fig. 1 Molecular structure of $[Cu(N,N)_2]PF_6$ (**1**). Thermal ellipsoids are shown with 30% probability. PF_6^- counter ion was omitted for clarity.

lengthening from 2.055(4) Å (Cu1–N3A); 2.038(4) Å (Cu1–N2A) in complex **1** to 2.073(6) Å (Cu1–N2); 2.121(6) Å (Cu1–N3) in complex **2**. In both complexes the diisopropylphenyl group is almost orthogonal to the plane formed by the indazole ring with a dihedral angle of 105.8(6)° (C12A–C11A–N3A–C8A) for complex **1** and 86.0(9)° (C12–C11–N3–C8) for complex **2**, giving the metal center a large steric hindrance, specially the phosphine ancillary ligand in complex **2**. For further information of bond distances and angles see the ESI.†

UV-Vis absorption spectra

Fig. 3 shows the UV-Vis absorption spectra of the four Cu(I) complexes $[Cu(N,N)_2]PF_6$ (**1**), $[Cu(N,N)(POP)]PF_6$ (**2**), $[Cu(N,N)(dppe)]PF_6$ (**3**), and $[Cu(N,N)(PPh_3)_2]PF_6$ (**4**) measured in CH_2Cl_2 solution at room temperature, while the absorption data are summarized in Table 2. The studied complexes **1–4** displayed electronic transitions similar to those of related Cu(I) complexes reported in the literature and their assignments were carried out accordingly.[9d,g,h,k,n,17]

Complexes **1–4** exhibit one intense absorption band with maxima between 292 and 309 nm; these absorption bands where assigned to $\pi \rightarrow \pi^*$ spin allowed transitions centered in the *N,N* ligand (LC) by means of comparison with the UV-Vis spectrum of the free and protonated *N,N* ligands (Fig. S1 of ESI†). At lower energies less intense and broad bands were observed, which were not found in the free ligand spectrum. In the case of complex $[Cu(N,N)_2]PF_6$ (**1**), this absorption appears

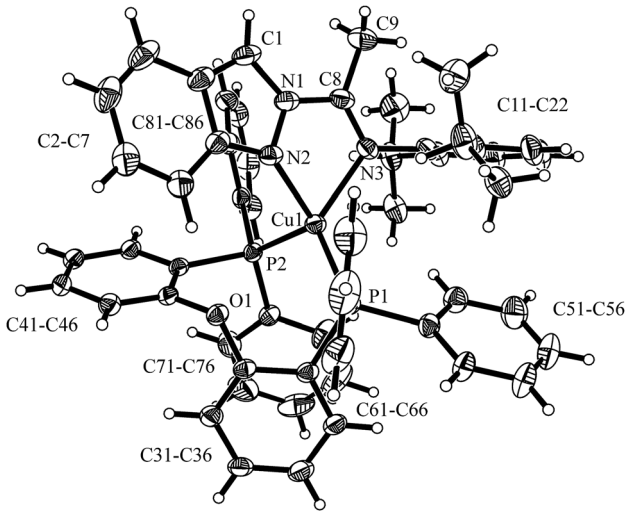

Fig. 2 Molecular structure of [Cu(*N*,*N*)(POP)]PF_6 (**2**). Thermal ellipsoids are shown with 30% probability. PF_6^- counter ion was omitted for clarity.

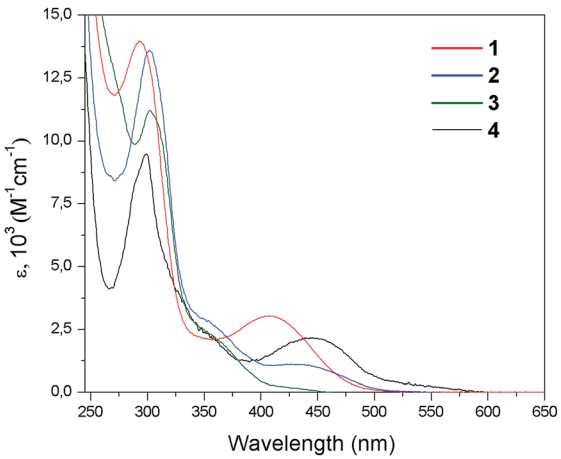

Fig. 3 Absorption spectra of complexes **1–4** in CH_2Cl_2 at room temperature.

with a maximum at 448 nm ($\varepsilon = 2.1 \times 10^3$ M^{-1} cm^{-1}) which can be assigned to a singlet metal-to-ligand charge transfer (^{1}MLCT) transition [Cu(d) → *N*,*N*(π*)].[5f,g,8] Furthermore, complex **1** shows a weak absorption in the range of 500–550 nm ($\varepsilon \sim 1 \times 10^3$ M^{-1} cm^{-1}), which is not present in complexes **2–4**. On the other hand, complexes **2–4** displays absorption bands at 408 nm ($\varepsilon = 3 \times 10^3$ M^{-1} cm^{-1}), 438 nm ($\varepsilon = 1.1 \times 10^3$ M^{-1} cm^{-1}), and 430 nm ($\varepsilon = 0.2 \times 10^3$ M^{-1} cm^{-1}), respectively. These absorption features are assigned to ^{1}MLCT transitions as observed for Cu(I) complexes involving aromatic diimine ligands.[9d,n] These ^{1}MLCT transitions mainly involve the 3d orbitals of the Cu(I) metal centers and the π* orbitals of the *N*,*N* ligands, specifically of the indazole fragment [Cu(d) → *N*,*N*(π*)], which are derived from the DFT calculations (*vide infra*).

The displacement of the ^{1}MLCT band throughout the **1–4** series is in agreement with the reported behavior of Cu(I) complexes.[8b,9d,18] Compared to complex **1**, complexes **2–4** show a blue shift of their MLCT bands (between 10 and 40 nm). This effect is mainly related to the stabilization of the HOMO of the complexes *via* the interactions of the Cu(I) centers with the phosphine ancillary ligands, whereas in these cases the LUMO remains practically unchanged. The computed HOMO and LUMO energies and the HOMO–LUMO energy gaps ($\Delta E_{(H-L)}$) are sketched in Fig. 4. It is noted that the LUMO energies are almost the same for all complexes (~−2.6 eV), in agreement with the small differences found among the electrochemical reduction potentials (see below Table 4). The latter is consistent with about 96% of the LUMO density delocalized on the *N*,*N* ligand for all the systems. On the other hand, the HOMO energy changes in a very sensitive way throughout the **1–4** series as expected on the basis of the different ligand environment (*N*,*N* *vs.* *P*,*P* ligands).

In particular, substitution of *N*,*N* ligand with a *P*,*P* ligand causes stabilization of the HOMO level, thus determining an increase of the $\Delta E_{(H-L)}$ values on going from the homoleptic complex **1** to the heteroleptic complexes **2–4**, which is in agreement with the electrochemical gaps (see below Table 4). Moreover, as for [Cu(*N*,*N*)(*P*,*P*)]PF_6 complexes, the spatial

Table 2 Photophysical data of complexes **1–4**

	Absorption		Emission[a]			
			KBr pellet[c]		PMMA film[c]	
Complex	CH_2Cl_2 λ_{max} [nm] (ε_{max} [M^{-1} cm^{-1}])	77[b] K λ_{max} [nm]	λ_{max} [nm]	Φ^d	λ_{max} [nm]	Φ^d
[Cu(*N*,*N*)$_2$]PF_6 (**1**)	298 (9.5×10^3) 448 (2.1×10^3) 500–550 (1×10^3)	580, 599, 632, 689	n.d.	n.d.	n.d.	n.d.
[Cu(*N*,*N*)(POP)]PF_6 (**2**)	292 (1.4×10^4) 408 (3.0×10^3)	603, 654, 714	625, 667	0.008	659	0.011
[Cu(*N*,*N*)(dppe)]PF_6 (**3**)	302 (1.4×10^4) 438 (1.1×10^3)	616, 667, 724	n.d.	n.d.	n.d.	n.d.
[Cu(*N*,*N*)(PPh_3)$_2$]PF_6 (**4**)	309 (1.1×10^4) 430 (2.0×10^2)	607, 658, 714	620, 657	0.004	650	0.008

[a] In CH_2Cl_2 at room temperature the complexes were not emissive. [b] 4/1 ethanol/methanol glassy matrix excitation at 440 nm in **1**, at 380 nm in **2–4**. [c] Excitation at 400 nm in 2 and at 380 nm in **4**. [d] Absolute quantum yields estimated using an integrating sphere set up. n.d. = not detected.

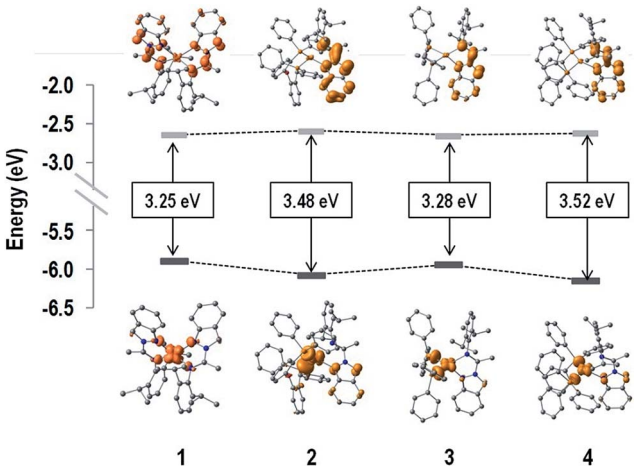

Fig. 4 HOMO and LUMO density surfaces, and HOMO–LUMO energy gaps ($\Delta E_{(H-L)}$) of complexes **1–4**. Hydrogen atoms were deleted for clarity.

arrangement of the phosphines around the metal center (bite angle, geometric constraint, and steric hindrance)[9a,14c] and, in the case of complex **4**, the rotation of the PPh_3 affects both the energy of the MLCT band as well as its intensity (ε). In particular, wider P–Cu–P bite angles should increase the MLCT absorption energy as a consequence of the variation in the d–σ* interactions.[9a,d] Indeed, this consideration can explain the lowest MLCT energy observed for complex **3** with respect to complexes **2** and **4** (Fig. 3 and Table 2), which correlates with the smallest P–Cu–P angle within the heteroleptic **2–4** series (111.1(3)° for complex **2** as obtained from X-ray analyses, 88.65° for complex**3** and 119.83° for complex **4** as obtained from DFT computations, see ESI†). This is also consistent with the smaller HOMO–LUMO gap estimated *via* DFT calculations as well as

Table 4 Redox potentials of Cu(I) complexes **1–4** from CV measurements[a]

	E_{Ox} [V]	E_{Red} [V]	$\Delta E_{(Ox-Red)}$ [V]	$\Delta E_{(H-L)}$[b] [eV]
$[Cu(N,N)_2]PF_6$ (**1**)	0.956	n.a.	—	3.25
$[Cu(N,N)(POP)]PF_6$ (**2**)	1.512	−1.107	2.619	3.48
$[Cu(N,N)(dppe)]PF_6$ (**3**)	1.239	−1.138	2.377	3.28
$[Cu(N,N)(PPh_3)_2]PF_6$ (**4**)	1.337	−1.231	2.568	3.52

[a] Potential measured at room temperature, in CH_2Cl_2 solution at a scan rate of 50 mV s^{-1}, *versus* Ag/AgCl electrode. [b] From DFT calculations, n.a. = not assigned.

with the smaller electrochemical gap (see below) observed for **3** with respect to complexes **2** and **4**. In addition, the increase in the geometric constraint of the phosphine is observed to influence the intensity of the MLCT absorption, with the molar absorptivity showing a progressive enhancement in the order PPh_3 < dppe < POP.

To gain further insight into the low-energy transitions of complexes **1–4**, the low-lying excited states were computed by means of time dependent DFT calculations (TD-DFT). Solvent effects were included by the PCM method[19] with CH_2Cl_2 as solvent. Table 3 summarizes the transition energies, single excitations (and contributions) and nature of the low-lying excited states of complexes **1–4**, and Fig. 5 depicts the hole and electron distributions.

In complex **1** the computed transition at 462 nm ($f = 0.111$) could be related to the intense experimental absorption band at lower energies, which results from an electron promotion from HOMO−1 → LUMO (0.63), and a small contribution from the HOMO → LUMO+1 (0.28) transition. Note that the HOMO (and HOMO−1) is mainly composed of 53% 3d orbital character from the metal core. In addition, significant contributions to HOMO (HOMO−1) from the *N*,*N* ligands are observed

Table 3 Properties of the low-lying singlet excited states of complexes **1–4**[a]

Complex	State	Absorption λ_{max} [nm] (E [eV])	f	Monoexcitations (CI coef. and % cont.)	Description of the electronic transition
1	S_1	513 (2.42)	0.029	H−1 → L (−0.28; 15%); H → L+1 (0.64; 81%)	Cu(d) + *N*,*N*(π) → *N*,*N*(π*); ^{1}MLCT/^{1}ILCT
	S_2	503 (2.46)	0.009	H−1 → L+1 (−0.35; 25%); H → L (0.60; 72%)	Cu(d) + *N*,*N*(π) → *N*,*N*(π*); ^{1}MLCT/^{1}ILCT
	S_3	462 (2.68)	0.111	H−1 → L (0.63; 80%); H → L+1 (0.28; 16%)	Cu(d) + *N*,*N*(π) → *N*,*N*(π*); ^{1}MLCT/^{1}ILCT
2	S_1	427 (2.90)	0.089	H → L (0.70; 98%)	Cu(d) + *P*,*P*(π) → *N*,*N*(π*); ^{1}MLCT/^{1}LLCT
	S_4	352 (3.52)	0.015	H−3 → L (0.52; 55%); H−2 → L (−0.43; 37%)	*N*,*N*(π) + *P*,*P*(π) → *N*,*N*(π*); ^{1}LLCT/^{1}ILCT
3	S_1	458 (2.70)	0.098	H → L (0.71; 98%)	Cu(d) + *P*,*P*(π) → *N*,*N*(π*); ^{1}MLCT/^{1}LLCT
	S_2	414 (3.00)	0.016	H−1 → L (0.69; 96%)	Cu(d) + *N*,*N*(π) → *N*,*N*(π*); ^{1}MLCT/^{1}ILCT
	S_3	358 (3.47)	0.026	H−2 → L (0.69; 96%)	*N*,*N*(π) → *N*,*N*(π*); ^{1}ILCT
4	S_1	419 (2.96)	0.082	H → L (0.70; 97%)	Cu(d) + *P*,*P*(π) → *N*,*N*(π*); ^{1}MLCT/^{1}LLCT
	S_2	400 (3.10)	0.014	H−1 → L (0.67; 91%)	Cu(d) + *N*,*N*(π) → *N*,*N*(π*); ^{1}MLCT/^{1}ILCT
	S_4	345 (3.59)	0.020	H−4 → L (−0.34; 24%); H−3 → L (0.59; 70%)	*N*,*N*(π) → *N*,*N*(π*); ^{1}ILCT

[a] E: transition energies, f: oscillator strength, CI: CI coefficient, % cont.: percentage of contribution to the excited state wave function, H: HOMO and L: LUMO.

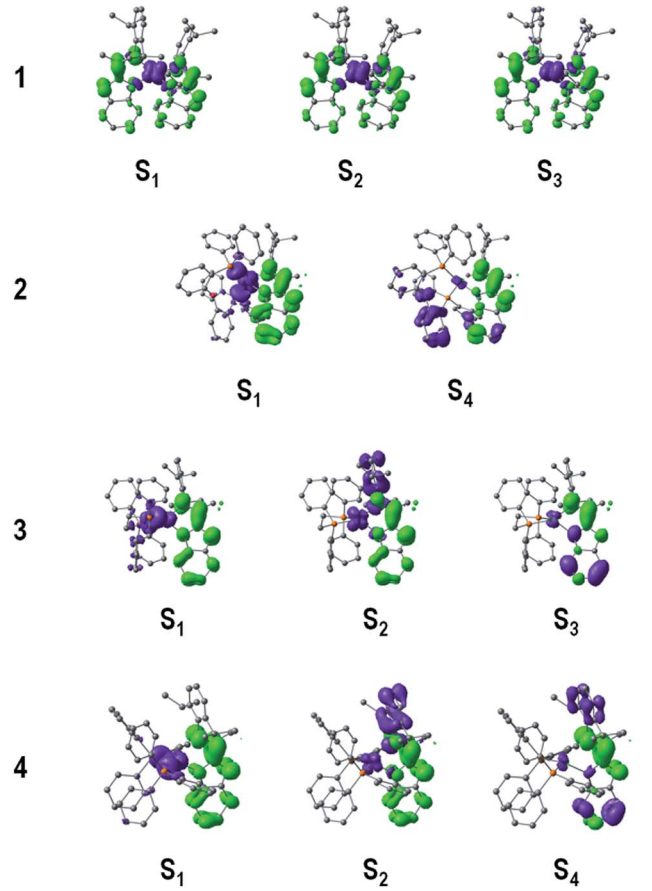

Fig. 5 Hole (purple) and electron (green) distributions of selected singlet excited states (S_i) of complexes **1–4**. Hydrogen atoms were deleted for clarity.

stemming from the p orbitals of the nitrogen atoms involved in the Cu–N bonds and the carbon atoms in the aniline rings, with values of 28% (34%) and 11% (18%) orbital contributions, respectively. In addition, LUMO and LUMO+1 are delocalized in the indazole moieties of the *N*,*N* ligands by ~88%. Therefore, the excited state at 462 nm is mainly assigned to a metal-to-ligand charge transfer (^{1}MLCT) transition [Cu(d) → *N*,*N*(π*)] with some intra-ligand charge-transfer character (^{1}ILCT) [*N*,*N*(π) → *N*,*N*(π*)], which is consistent with the hole–electron distribution shown in Fig. 5. Furthermore, poorly intense transitions at 513 ($f = 0.029$) and 503 nm ($f = 0.01$) display the same ^{1}MLCT/^{1}ILCT character, and are assigned to the weak band of the experimental spectrum falling in the range of 500–550 nm for complex **1**.

The heteroleptic complexes **2–4** exhibit the HOMO−*n* → LUMO transitions in the range of 350–450 nm, where the LUMO is mainly consisting of π* orbitals of the indazole part of the *N*,*N* ligand. The first singlet excited state of complex **2** appears at 427 nm ($f = 0.09$), in good agreement with the experimental data; this HOMO → LUMO transition displays a mixed ^{1}MLCT and ^{1}LLCT character [Cu(d) + POP(π) → *N*,*N*(π*)], since the HOMO of complex **2** is localized mainly on the metal center (31%) and on the *P*,*P* ligand (POP) (48%).

Unlike for systems **1** and **2**, the experimental UV-Vis spectrum of complex **3** displays a shoulder structure between 350 and 500 nm and the TD-DFT calculations confirms this interpretation. The band at lower energies (458 nm, $f = 0.098$) is due to a HOMO → LUMO transition with a mixed ^{1}MLCT/^{1}LLCT character [Cu(d) + dppe(π) → *N*,*N*(π*)]. This excited state involves an electron transition from the metal center and the *P*,*P* ligand (dppe) [where the HOMO resides: Cu (32%) and dppe (54%)] to the indazole part of the *N*,*N* ligand. In addition, a S_2 excited state of ^{1}MLCT/^{1}ILCT character [Cu(d) + *N*,*N*(π) → *N*,*N*(π*)] is computed at 414 nm ($f = 0.016$), which shows a smaller oscillator strength compared to the S_1 state explaining the broad low-intensity experimental band between 400 and 450 nm. In addition, a ^{1}ILCT (π → π*) transition (centered in the indazole part of the *N*,*N* ligand) is found at higher energies for complex **3** causing the shoulder at ~358 nm.

Finally, complex **4** revealed similar absorption band features as complex **3** in the range of 350–400 nm, but with lower ε values, which was attributed to the high degree of freedom and vibrational character of the PPh_3 groups in solution. The latter is consistent with the S_1 state (HOMO → LUMO) computed at 419 nm ($f = 0.082$), where the HOMO is mainly localized at the *P*,*P* ligand (48%) and in part at the metal center (28%), thus this transition is expected to be observed with a low intensity due to the rotational character of the PPh_3 ligands. Moreover, the S_2 and S_4 states show the same electronic structure as for **3**, which posses a larger ligand-centered character involving mainly the *N*,*N* ligand (>67%).

Electrochemical properties

The electrochemical properties of the complexes were determined by cyclic voltammetry in dichloromethane solution and the data are summarized in Table 4. Complex **1** shows the lowest oxidation potential (0.956 V) of all complexes. This oxidation is associated to the irreversible Cu(II)/Cu(I) processes.[9h,20] Unfortunately, the reduction processes of complex **1** could not be assigned due to a poorly resolved shoulder peak. Presumably, this broad reduction peak likely involves multiple electron-transfer and a fast kinetic ligand reduction.[21]

Complex **2** exhibits the higher oxidation potential (1.512 V) within the **1–4** series, revealing the better π acceptor character of the POP ligand over the *N*,*N* ligand. For complexes **3** and **4**, irreversible anodic processes were observed at potentials of 1.239 V and 1.337 V, respectively, associated to the Cu(II)/Cu(I) couple; this difference is mainly due to the effect of the different *P*,*P* ligands on the metal center. On the other hand, the cathodic processes observed for complexes **2–4** fall at similar potential values, in agreement with the similar LUMO energies obtained from DFT calculations (see Fig. 4). Also, these results are consistent with the MLCT energy values observed in the absorption spectra of the complexes. For instance, complexes **2** and **4** exhibit the highest $\Delta E_{(Ox-Red)}$ and $\Delta E_{(H-L)}$, thus they show the greatest blue shift in the absorptions spectrum.

Luminescence properties

At room temperature in deaerated CH_2Cl_2 solution all the four complexes are not emissive. Therefore, the luminescent properties of all complexes were studied in the solid state at 77 K (4 : 1 ethanol : methanol glassy matrix), in KBr pellet, and in a PMMA film.[22,23] The results are depicted in Fig. 6 and the data summarized in Table 2.

In the rigid matrix at 77 K, complex **1** displays a structured emission with relative maxima at 580, 599, 632 nm, which are considerably blue-shifted when compared to the related emissions of complexes **2–4**, the luminescence of which has a structured profile featuring three different maxima (at 603, 654, 714 nm for **2**, at 616, 667, 624 nm for **3**, and 607, 658, 714 nm for **4**, see Table 2), thus suggesting a similar character of the emitting state throughout the **2–4** series. Interestingly, the spectra of complexes **2–4** shown in Fig. 6a resemble the phosphorescence spectrum of the protonated *N*,*N* ligand (Fig. S2 of the ESI†). This clearly means that for **2–4** the emitting state at 77 K is mainly of ligand-centered (LC) character, whereas in the case of **1** a mixed MLCT/LC emission is most likely responsible for the differences in the structure of the luminescence profiles. The appreciable blue-shift of the emission of **1** with respect to those of **2–4** is also consistent with this notion. These findings can be rationalized considering the destabilization of the triplet MLCT excited state with respect to the ligand-centered triplet excited state occurring in the 77 K rigid medium. This destabilization is considerably larger in the case of the heteroleptic compounds **2–4** rather than for the homoleptic complex **1** as a result of the electronic effects exerted by the phosphine-based ligands.

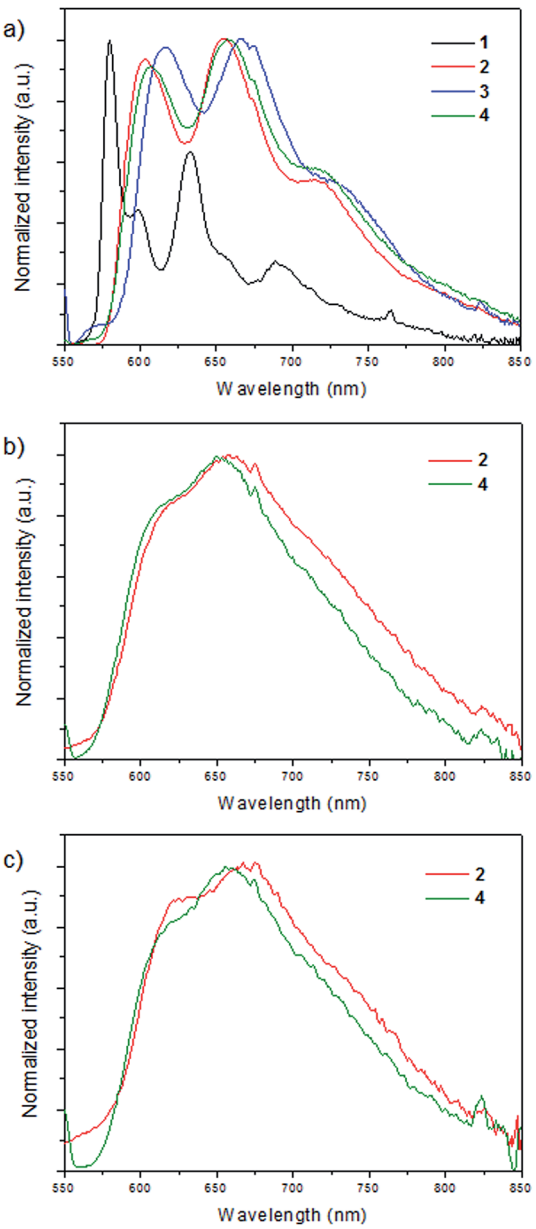

Fig. 6 Normalized emission spectra of: (a) complexes **1–4** at 77 K in a 4 : 1 ethanol : methanol glassy matrix, (b) complexes **2** and **4** in PMMA film at room temperature, (c) complexes **2** and **4** in KBr pellet at room temperature.

In the solid state at room temperature, both in a PMMA film and a KBr pellet, emission is detected only for compounds **2** and **4** (Fig. 6b and c) with quantum yields between 0.004 and 0.011 (see Table 2). Complexes **1** and **3** display negligible photoluminescence. The emission profile for both complexes and in both matrices features a band with maximum at *ca.* 650 nm and a shoulder in the blue which is comparable in terms of both shape and energy with the structured emission observed in the glassy matrix at 77 K. This suggests that emission at room temperature of complexes **2** and **4** is mainly of ligand-centered (^{3}LC) character, in agreement with the destabilization of the MLCT excited state that take place in the solid state.

The most likely explanation for the negligible emission originating from the excitation of complexes **1** and **3**, either in PMMA film or KBr pellet, is that thermal population of the closely-lying ^{3}MLCT excited state may take place at room temperature and non-radiative deactivation may become more favorable with respect to the 77 K glassy matrix (where an MLCT contribution is indeed observed in the emission of **1**). This is correlated to the lower energies of the ^{3}MLCT state in compounds **1** (homoleptic complex) and **3** (due to the smallest P–Cu–P angle within the heteroleptic complexes) with respect to complexes **2** and **4**, consistently with both the absorption and electrochemical data as well as with the theoretical calculations.

DFT calculations of the first triplet excited states (T_1) (at its optimized geometries) confirmed the nature of the emissive states. Fig. 7 shows the T_1 spin densities of compounds **1–4**. Note that in the triplet electronic states, two unpaired electrons are found and the spin densities sum up to the total of unpaired electrons. In the case of complex **1**, the unpaired electrons are mainly localized on the *N*,*N* ligand (1.61e) with a minor contribution from the metal core (0.39e) indicating that the nature of the T_1 transition is ~80% of ^{3}LC, while the ^{3}MLCT contribution is only about 20%, which is in agreement with the experimental findings. On the other hand, in compounds **2–4** the metal contributions of the T_1 states are only ~10%, clearly indicating that their emissive states are mainly involving the ^{3}LC states as explained from the experimental results. Then the low ^{3}MLCT contributions decrease the spin orbit coupling and

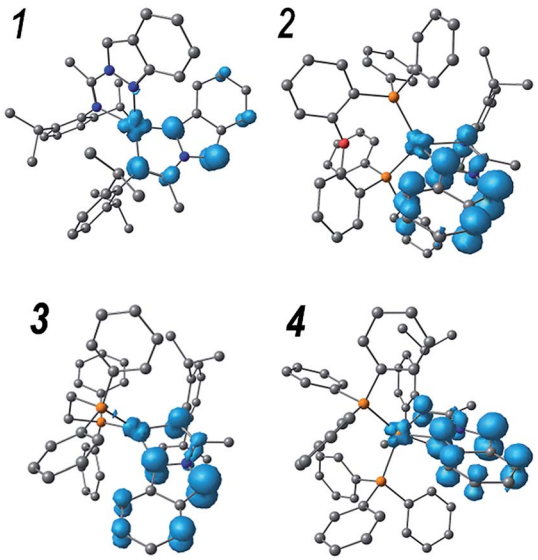

Fig. 7 Spin density surfaces of the optimized first triplet excited state (T_1) of complexes **1–4**.

consequently the luminescence efficiency. Specifically, the spin densities in the metal core appear to be 0.12, 0.20 and 0.30e for compounds **2**, **3** and **4**, respectively, while in the *N*,*N* ligands values of 1.75, 1.60 and 1.74e are found, respectively.

Transient absorption spectroscopy

In order to acquire deeper understanding of the photophysical properties, transient absorption spectroscopy studies were performed on complexes **1–4**. Laser flash photolysis studies have been first applied to the whole series of complexes spanning a time window from ns to ms. Whereas the homoleptic complex **1** does not display any transient signal upon 355 nm excitation in CH_2Cl_2 solution (*vide infra*), the heteroleptic complexes **2–4** show similar transient signatures. Going into more detail, a transient species is immediately observed after the laser pulse in the case of complex **2**. Its spectrum (Fig. 8) features an absorption centered at 490 nm with a tail at longer wavelengths. This spectrum decays monotonically to the baseline with oxygen-dependent kinetics (τ = 760 ns under aerated conditions, Fig. S3 of ESI,† and τ = 19.9 μs under degassed conditions, Fig. S4 of ESI†) clearly confirming the triplet character of the transient species. The presence of an apparent bleaching at ~400 nm is consistent with the depletion of the MLCT absorption in the excited state. However, the considerably long lifetime in the absence of any detectable emission at room temperature, clearly suggests a strong contribution from a ligand-centered triplet excited state (^{3}LC) consistent with the photoluminescence data. Therefore these observations point towards a mixed ^{3}MLCT/^{3}LC character of the transient species in **2** undergoing non-radiative deactivation in the μs time-scale.

As far as complex **3** is concerned, the transient spectrum detected in the ns time-scale is depicted in Fig. 9. It displays a broad absorption centered at *ca.* 480 nm with a tail at longer wavelengths, very similar to the ones observed for the remaining heteroleptic complexes (Fig. 8 for **2** and see below Fig. 10 for **4**), thus suggesting a similar character of the transient species.

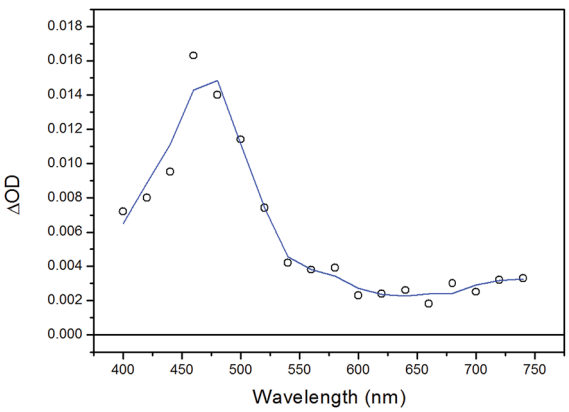

Fig. 9 Transient absorption spectra of complex **3** in CH_2Cl_2 obtained by laser flash photolysis (excitation at 355 nm, FWHM = 6–8 ns) at 30 ns time delay.

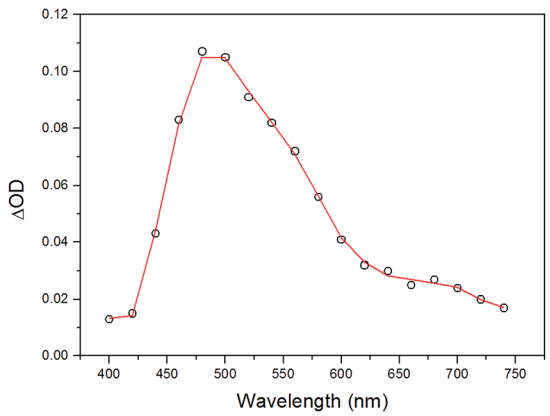

Fig. 8 Transient absorption spectrum of complex **2** in CH_2Cl_2 obtained by laser flash photolysis (excitation at 355 nm, FWHM = 6–8 ns) at 20 ns time delay.

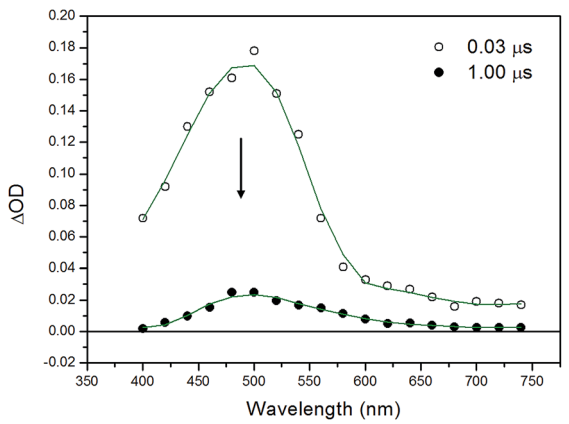

Fig. 10 Transient absorption spectra of complex **4** in CH_2Cl_2 obtained by laser flash photolysis (excitation at 355 nm, FWHM = 6–8 ns) at 30 ns time delay (empty dots) and at 1 μs time delay (full dots).

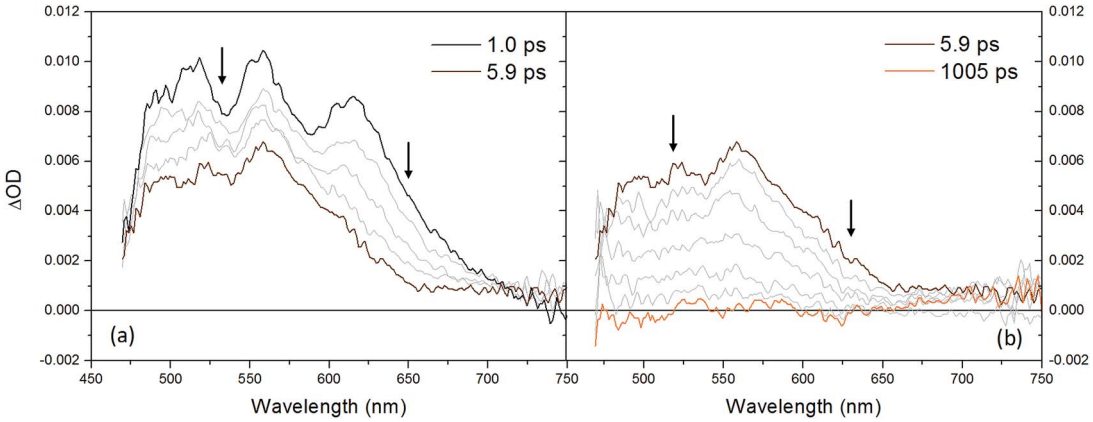

Fig. 11 Transient absorption spectra obtained by ultrafast spectroscopy (excitation wavelength $\lambda = 400$ nm) of complex **1** in CH_2Cl_2 between (a) 1.0–5.9 ps and (b) 5.9–1005 ps.

On the other hand, an interesting difference is observed as far as the kinetics of the transient absorption decay is concerned. The transient species indeed decays with oxygen dependent kinetics with a lifetime of $\tau = 540$ ns under air-equilibrated conditions (Fig. S5 of ESI†) and $\tau = 960$ ns after oxygen removal (Fig. S6 of ESI†). The elongation of the lifetime is consistent with the triplet character of the deactivating excited state. However, the small entity of the lifetime elongation (compared with what observed for complexes **2** and **4**, see below) may suggest that the degree of ^{3}LC/^{3}MLCT mixing is lower and the deactivating species most likely displays a larger ^{3}MLCT character than in the case of complexes **2** and **4**. In this situation, the higher contribution of the metal center in the excited state would increase the spin–orbit coupling thus fostering a faster excited state decay. The reasons for this different behavior may lie on the stereoelectronic effect exerted by the dppe ancillary ligand which, as stated above, forces a smaller P–Cu–P angle with respect to the POP and PPh_3 ligands, thus lowering the MLCT energy.

Regarding complex **4**, the excited state dynamics is biphasic in nature. Indeed, the transient spectrum, which is detected immediately after the laser pulse (Fig. 10, black trace), featuring an intense absorption with a maximum at 500 nm with a tail at longer wavelengths, is observed to undergo a fast decay (time-constant of $\tau = 91$ ns, Fig. S7 of ESI†) yielding a transient spectrum with similar spectral characteristics (Fig. 10, red trace), only differing from the former in the presence of a more intense bleaching at $\lambda < 450$ nm and a more accentuated absorption tail at $\lambda > 550$ nm (see the comparison of the normalized spectra in Fig. S8 of ESI†). This transient signal then decays to the baseline with oxygen-dependent kinetics ($\tau = 635$ ns under aerated conditions, Fig. S7 of ESI,† $\tau = 37.7$ μs under degassed conditions, see Fig. S9 of ESI†), supporting the triplet nature of the deactivating excited state. Similarly to complex **2**, the spectral shape of the deactivating transient signal, as well as the observed long lifetime strongly suggests a mixed ^{3}MLCT/^{3}LC character of the transient species in **4**. A slow thermal equilibration between the ^{3}MLCT and the ^{3}LC excited states,[23] or a competitive parallel deactivation from a different, closely-lying excited state level may account for the faster decaying component.‡

As previously mentioned, no transient processes have been observed in the ns time-scale, as far as the homoleptic complex **1** is concerned. Therefore, in order to clarify the excited state behavior of **1** ultrafast transient absorption spectroscopy studies have been undertaken. The excited state dynamics is shown in Fig. 11 and can be split into two different processes. The first process (Fig. 11a) involves the evolution of a structured spectrum (sampled at a time-delay $\tau = 1$ ps) with three distinct maxima at 520, 555, and 615 nm to a featureless spectrum with a broad absorption (maximum at 560 nm) and takes place with a time-constant of $\tau = ca.$ 2 ps (Fig. S10 of ESI†). The second process (Fig. 11b) is defined by the monotonic decay of this broad transient spectrum to the baseline and occurs with a time-constant of $\tau = ca.$ 280 ps (Fig. S10 of ESI†). The prompt transient spectrum with its multi-peak characteristic can be very likely attributed to the localized singlet MLCT excited state, stabilized after sub-picosecond flattening distortion.[24] The presence of an apparent bleaching at $\lambda < 480$ nm is consistent with the MLCT depletion in the excited state. As a consequence, the first process ($\tau = ca.$ 2 ps) can be ascribed to the fast singlet-triplet intersystem crossing, mainly dictated by the spin–orbit coupling promoted by the heavy copper center (MLCT bleaching is indeed still retained after the fast process). Finally, the second process ($\tau = ca.$ 280 ps) corresponds to the decay of the triplet MLCT excited state to the ground state.

In general, the observed different lifetimes (*e.g.*, the smaller one measured in **1** with respect to the remaining complexes **2–4** and the slight difference observed in **3** with respect to complexes **2** and **4**) are intimately connected to the different character of the lowest lying excited state, namely pure ^{3}MLCT and mixed ^{3}LC/^{3}MLCT, and the degree of mixing between the latters, which is determined by the different electronic effects

‡ Laser flash photolysis experiments at different excitation power clearly rule out triplet–triplet annihilation processes being responsible for the faster decaying component.

played by the presence or absence of the ancillary *P*,*P* ligand, as well as their steric constraint.

Conclusions

A series of new mixed ligands Cu(I) complexes (**1–4**) were prepared *via* a simple synthetic route of ligand exchanges with high yields. The X-ray single crystal characterization of complexes **1** and **2** showed that the Cu(I) metal centers have a pseudo-tetrahedral geometries with a highly congested environment. The photophysical properties of complexes **1–4** were also successfully investigated. The four complexes exhibited MLCT absorption bands in the UV-Vis spectra in the range 400–450 nm, with energies and intensities dependent on the type of coordinated ligand. At room temperature the four weakly luminescent in a glassy matrix at 77 K. In the glassy matrix, complex **1** displayed a structured emission, which was considerably blue-shifted when compared to the emission of complexes **2–4**. The luminescence of the latter was similar and resembled the luminescence of the protonated *N*,*N* ligand thus indicating a large contribution from a ^{3}LC excited state.

The negligible emissions of complexes **1** and **3**, at room temperature in the solid state (PMMA film or KBr pellet), suggest thermally activated deactivation processes instead of complexes **2** and **4** that show a weak ligand-centered emission with quantum yields between 0.004 and 0.011.

Furthermore, transient absorption spectroscopy studies were exploited to follow the decay of the lowest lying excited states at room temperature. While complex **1** displayed a fast decay of the ^{3}MLCT excited state to the ground state occurring with a lifetime of τ = *ca.* 280 ps, complexes **2–4** showed considerably long lifetimes in the μs time scale, which in the absence of any detectable emission, clearly suggested a mixed ^{3}MLCT/^{3}LC character of the transient species with a strong contribution arising from a ligand-centered (LC) triplet excited state, consistent with the photoluminescence data at 77 K.

Although complexes **1–4** are not emissive in CH_2Cl_2 solution, the observed emission in a rigid medium shows us that complex **2**, bearing POP phosphine ancillary ligand, has the better structural and photophysical properties. In conclusion, based on the deep photophysical study performed, we can deduce that Cu(I) heteroleptic complexes with *N*,*N* imidoyl-indazole derivative ligands and POP phosphine can be potentially exploited as cheap materials for LEEC devices. Further efforts in the research towards the synthesis and applications of Cu(I) heteroleptic complexes, with small changes in the molecular structure of the *N*,*N* ligand and using the POP phosphine, are necessary for the improvement of the observed properties and these are currently ongoing in our laboratory.

Experimental

General remarks

All reagents were purchased from Sigma-Aldrich and used as received, unless otherwise specified. *N*,*N* ligand was prepared as described in the literature.[15] NMR spectra were recorded on NMR Bruker AV 400. Chemical shifts are given in parts per million relative to TMS [^{1}H and ^{13}C, $\delta(SiMe_4) = 0$] or an external standard [$\delta(BF_3OEt_2) = 0$ for ^{11}B NMR, $\delta(CFCl_3) = 0$ for ^{19}F NMR]. Most NMR assignments were supported by additional 2D experiments. Elemental analysis data were recorded on a Foss-Heraeus CHNO-Rapid analyzer. For Mass spectra were obtained on an HP 5988A spectrometer (Hewlett-Packard, Palo Alto, CA, USA). FT-IR spectra were recorded on a Bruker Vector-22 Spectrophotometer using KBr pellets. Electrochemical measurements were performed at a CHI730E potentiostat in a conventional three-compartment, three-electrode cell. Thin layer chromatography (TLC) was performed using Merck GF-254 type 60 silica gel. Column chromatography was carried out using Merck silica gel 60 (70–230 mesh). UV-Vis absorption spectra were recorded on a Jasco V-570 UV/Vis/NIR spectrophotometer. Photoluminescence spectra were taken on an Edinburgh Instrument spectrofluorimeter. Dichloromethane solutions of the complexes were previously degassed with N_2 for approximately 20 min. KBr pellets containing complexes **1–4** were prepared by grinding the solid sample with solid potassium bromide purchased from Sigma-Aldrich. Poly(methyl methacrylate) (PMMA) films were prepared from CH_2Cl_2 solutions of **1–4** and low molecular weight poly(methyl methacrylate) followed by drop casting onto a glass surface. In both cases the concentration was adjusted depending on the absorption coefficient of the sample. The thickness of the polymeric film was not controlled. Femtosecond time-resolved experiments were performed using a pump–probe setup based on the Spectra-Physics Hurricane Ti:sapphire laser source and the Ultrafast Systems Helios spectrometer. The time-resolved spectral data were analyzed with the Ultrafast Systems Surface Explorer Pro software. Nanosecond transient measurements were performed with a custom laser spectrometer comprised of a Continuum Surelite II Nd : YAG laser (FWHM = 6–8 ns). For X-ray crystal structure analysis, data sets were collected with a Nonius Kappa CCD diffractometer; full details can be found in the independently deposited crystallography information files (cif), CCDC numbers: 1422058 for compound **1** and 1422059 for compound **2**.†

DFT calculations

DFT calculations were performed in the Gaussian 09 program with the B3LYP[25] functional. The 6-31G(d,p) basis set was used for H, C, N, O and F atoms; the quasi-relativistic pseudopotential and basis set LANL2DZ[26] was adopted for the metal. Ground states were fully optimized without symmetry restrictions, and vibrational frequencies were obtained in order to insure that optimized structures correspond to energy minimum, obtaining only positive frequencies. At the TD-DFT methodology, the first fifty singlet excited states were obtained to account for the characteristics of the experimental UV-Vis spectrum. Solvent effects were included by the PCM method,[19,27] with dichloromethane as solvent. Hole–electron distributions and molecular orbital compositions were obtained by the Multiwfn code.[28]

Synthesis of complexes

Complex 1. A solution of $[Cu(CH_3CN)_4]PF_6$ (233 mg, 0.63 mmol) in dichloromethane was added dropwise to a solution of

(1-(2*H*-indazol-2-yl)ethylidene)-2,6-diisopropylaniline[15] (400 mg, 1.25 mmol) in dry dichloromethane. The reaction mixture was stirred for 2 hours at room temperature. Then, the volatiles were removed in vacuum. Crude product was purified by crystallization. Obtaining **1** as a deep red crystalline material in 94% yield (499 mg, 0.59 mmol). Single crystals for X-ray crystallography were grown by layering pentane onto a toluene solution of compound 1 at −30 °C. ^{1}H NMR (400 MHz, CD_2Cl_2, 298 K): δ/ppm = 8.80 (s, 1H), 7.73 (d, J = 8.5 Hz, 1H), 7.22 (t, J = 7.3 Hz, 1H), 7.02 (m, 5H), 2.79 (broad, 2H), 2.46 (s, 3H), 1.00 (d, J = 6.7 Hz, 6H), 0.34 (broad, 6H). ^{13}C{^{1}H} NMR (100 MHz, CD_2Cl_2, 298 K): δ/ppm = 157.4, 147.6, 140.9, 139.3, 131.8, 127.3, 125.4, 125.1, 124.8, 124.1, 122.5, 116.3, 28.8, 23.5, 22.9, 16.1. ^{19}F NMR (400 MHz, CD_2Cl_2, 298 K): δ/ppm = −72.6 (d, J^{F-P} = 710 Hz). ^{31}P{1H} NMR (160 MHz, CD_2Cl_2, 298 K): δ/ppm = −144.3 (hept, J^{P-F} = 710 Hz, PF_6). Elemental analysis (%) $C_{42}H_{50}CuF_6N_6P$ (M = 847.40 g mol^{-1}): calculated C 59.53, H 5.95, N 9.92; found C 59.32, H 6.57, N 10.18. HRMS-ESI: ($C_{42}H_{50}CuN_6$ [M]$^+$) calc: 701.3393; found: 701.3356. For additional 2D NMR spectrum and assignments data see ESI.†

Complex 2. A solution of (1-(2*H*-indazol-2-yl)ethylidene)-2,6-diisopropylaniline[15] (50 mg, 0.16 mmol) in acetonitrile was added dropwise to a solution of $[Cu(CH_3CN)_4]PF_6$ (58 mg, 0.16 mmol) in acetonitrile. The reaction mixture was stirred for 30 minutes at room temperature. Then, a solution of (oxydi-2,1-phenylene)bis(diphenyl phosphine) (POP) (84 mg, 0.16 mmol) was added in acetonitrile and was stirred for 90 minutes at room temperature. The volatiles were removed in vacuum. Crude product was purified by crystallization using CH_2Cl_2/hexane mixture at −20 °C, resulting **2** as a yellow crystalline material in 98% yield (163 mg, 0.15 mmol). ^{1}H NMR (400 MHz, CD_2Cl_2, 298 K): δ/ppm = 9.06 (s, 1H), 7.84 (d, J = 8.6 Hz, 1H), 7.39 (t, J = 7.5 Hz, 1H), 7.27 (m, 8H), 7.14 (d, J = 7.8 Hz, 2H), 7.11 (m, 2H), 7.05 (m, 9H, H13), 6.88 (t, J = 7.2 Hz, 1H), 6.81 (m, 3H), 6.70 (broad, 4H), 6.47 (broad, 2H), 2.59 (hept, J = 6.5 Hz, 2H), 2.54 (s, 3H), 0.62 (d, J = 6.1 Hz, 6H), 0.49 (d, J = 6.1 Hz, 6H). ^{13}C{^{1}H} NMR (100 MHz, CD_2Cl_2, 298 K): δ/ppm = 158.0 (t, J^{C-P} = 5.7 Hz), 157.3, 149.4, 142.1, 139.6, 135.1 (t, J^{C-P} = 8.5 Hz), 134.5, 133.0 (t, J^{C-P} = 7.9 Hz), 132.3, 131.7, 131.1, 130.8, 129.6 (t, J^{C-P} = 4.8 Hz), 126.2, 125.4, 125.3, 125.1, 124.5, 122.2, 117.1, 28.9, 24.6, 22.9, 17.9. ^{19}F NMR (400 MHz, CD_2Cl_2, 298 K): δ/ppm = −72.9 (d, J^{F-P} = 710 Hz). ^{31}P{1H} NMR (160 MHz, CD_2Cl_2, 298 K): δ/ppm = −12.0 (s, POP), −144.3 (hept, J^{P-F} = 710 Hz, PF_6). Elemental analysis (%) $C_{57}H_{53}CuF_6N_3OP_3$ (M = 1066.51 g mol^{-1}): calculated C 64.19, H 5.01, N 3.94; found C 63.93, H 5.42, N 4.44. HRMS-ESI: ($C_{57}H_{53}CuN_3OP_2$ [M]$^+$) calc: 920.2960; found: 920.2916. For additional 2D NMR spectrum and assignments data see ESI.†

Complex 3. A solution of (1-(2*H*-indazol-2-yl)ethylidene)-2,6-diisopropylaniline[15] (50 mg, 0.16 mmol) in acetonitrile was added dropwise to a solution of $[Cu(CH_3CN)_4]PF_6$ (58 mg, 0.16 mmol) in acetonitrile. The reaction mixture was stirred for 30 minutes at room temperature. Then, a solution of 1,2-bis(diphenylphosphino)ethane (dppe) (62 mg, 0.16 mmol) was added in acetonitrile and was stirred for 90 minutes at room temperature. The volatiles were removed in vacuum. Crude product was purified by crystallization using CH_2Cl_2/hexane mixture and cold, obtaining **3** as a dark yellow solid in 95% yield (137 mg, 0.14 mmol). ^{1}H NMR (400 MHz, CD_2Cl_2, 298 K): δ/ppm = 9.06 (s, 1H, H9), 7.97 (d, J = 8.1 Hz, 1H, H14), 7.46 (m, 4H, H20), 7.38 (m, 1H, H6), 7.33 (m, 1H, H13), 7.28 (m, 2H, H5), 7.23 (m, 8H, H19), 7.15 (m, 9H, H11, H18), 2.81 (m, 2H, H2), 2.71 (s, 3H, H8), 2.31 (s, 4H, H16), 1.16 (d, J = 6.2 Hz, 6H, H1′), 0.80 (d, J = 6.2 Hz, 6H, H1). ^{13}C{^{1}H} NMR (100 MHz, CD_2Cl_2, 298 K): δ/ppm = 160.3 (C7), 149.8 (C15), 140.2 (C3), 139.0 (C4), 134.6 (C13), 133.1 (t, J^{C-P} = 7.5 Hz, C18), 132.4 (C20), 130.2 (t, J^{C-P} = 5.1 Hz, C19), 129.3 (t, J^{C-P} = 23 Hz, C17), 128.9 (C9), 128.3 (C6), 125.2 (C5), 124.4 (C10), 123.7 (C14), 115.7 (C11), 29.4 (C2), 24.7 (t, J^{C-P} = 16.2 Hz, C16), 23.7 (C1), 23.4 (C1′), 15.8 (C8). ^{19}F NMR (400 MHz, CD_2Cl_2, 298 K): δ/ppm = −72.7 (d, J^{F-P} = 710 Hz). ^{31}P{1H} NMR (160 MHz, CD_2Cl_2, 298 K): δ/ppm = 7.4 (s, dppe), −144.4 (hept, J^{P-F} = 710 Hz, PF_6). Elemental analysis (%) $C_{47}H_{49}CuF_6N_3P_3$ (M = 926.37 g mol^{-1}): calculated C 60.94, H 5.33, N 4.54; found C 60.30, H 4.85, N 5.02. HRMS-ESI: ($C_{47}H_{49}CuN_3P_2$ [M]$^+$) calc: 780.2698; found: 780.2669. For additional 2D NMR spectrum and assignments data see ESI.†

Complex 4. A solution of (1-(2*H*-indazol-2-yl)ethylidene)-2,6-diisopropylaniline[15] (50 mg, 0.16 mmol) in acetonitrile was added dropwise to a solution of $[Cu(CH_3CN)_4]PF_6$ (58 mg, 0.16 mmol) in acetonitrile. The reaction mixture was stirred for 30 minutes at room temperature. Then, a solution of triphenylphosphine (PPh_3) (82 mg, 0.31 mmol) was added in acetonitrile and was stirred for 90 minutes at room temperature. The volatiles were removed in vacuum. Crude product was purified by crystallization using cold tetrahydrofuran, obtaining **4** as a dark yellow solid in 92% yield (151 mg, 0.14 mmol). ^{1}H NMR (400 MHz, CD_2Cl_2, 298 K): δ/ppm = 9.22 (s, 1H), 7.94 (d, J = 8.4 Hz, 1H), 7.42 (m, 1H), 7.39 (t, J = 7.0 Hz, 4H), 7.24 (d, J = 7.8 Hz, 2H), 7.18 (m, 1H), 7.15 (t, J = 7.8 Hz, 8H), 7.08 (t, J = 7.6 Hz, 1H), 6.90 (t, J = 9.1 Hz, 8H), 6.72 (d, J = 8.8 Hz, 1H), 2.68 (s, 3H), 2.53 (hept, J = 6.7 Hz, 2H), 0.72 (d, J = 6.7 Hz, 6H), 0.37 (d, J = 6.7 Hz, 6H). ^{13}C{^{1}H} NMR (100 MHz, CD_2Cl_2, 298 K): δ/ppm = 158.0, 149.4, 141.6, 140.2, 134.1 (d, J^{C-P} = 14.8 Hz), 132.2 (d, J^{C-P} = 31.5 Hz), 131.9, 131.1, 129.5 (d, J^{C-P} = 9.4 Hz), 127.9, 127.4, 125.4, 125.3, 124.4, 122.8, 116.3, 29.1, 24.5, 23.2, 18.1. ^{19}F NMR (400 MHz, CD_2Cl_2, 298 K): δ/ppm = −72.8 (d, J^{F-P} = 710 Hz). ^{31}P{1H} NMR (160 MHz, CD_2Cl_2, 298 K): δ/ppm = 1.3 (s, PPh_3), −144.3 (hept, J^{P-F} = 710 Hz, PF_6). Elemental analysis (%) $C_{57}H_{55}CuF_6N_3P_3$ (M = 1052.52 g mol^{-1}): calculated C 65.04, H 5.27, N 3.99; found C 64.52, H 6.39, N 4.04. For additional 2D NMR spectrum and assignments data see ESI.†

Acknowledgements

Financial support from FONDECYT projects No. 1130077 and Millennium Science Initiative (ICM, Chile) for support through the Millennium Nucleus of Chemical Processes and Catalysis (CPC), project NC120082. A. C. is grateful for a postdoctoral fellowship, FONDECYT 3140425. I. G. is grateful for a postdoctoral fellowship, FONDECYT 3160285. H. B. gratefully acknowledges support from the University of Zurich, Switzerland. M. N. gratefully acknowledges FIRB RBAP11C58Y ''NanoSolar'' for funding.

Notes and references

1 (*a*) F. So, J. Kido and P. Burrows, *MRS Bull.*, 2008, **33**, 663; (*b*) Y. Chi and P.-T. Chou, *Chem. Soc. Rev.*, 2010, **39**, 638.

2 (*a*) Y.-L. Loo and J. McCulloch, *MRS Bull.*, 2008, **33**, 653; (*b*) U. Mitschke and P. J. Bäuerle, *Mater. Chem.*, 2000, **10**, 1471; (*c*) H. Yersin, *Highly Efficient OLEDs with Phosphorescent Materials*, Wiley-VCH, Weinheim, Germany, 2008.

3 (*a*) Y. You and S. O. Park, *Dalton Trans.*, 2009, 1267; (*b*) E. Holder, B. M. W. Langeveld and U. S. Schubert, *Adv. Mater.*, 2005, **17**, 1109; (*c*) L. He, J. Qiao, L. Duan, G. Dong, D. Zhang, L. Wang and Y. Qiu, *Adv. Funct. Mater.*, 2009, **19**, 2950; (*d*) T. Tsuzuki and S. Tokito, *Adv. Mater.*, 2007, **19**, 276; (*e*) C.-H. Yang, Y.-M. Cheng, Y. Chi, C.-J. Hsu, F.-C. Fang, K.-T. Wong, P.-T. Chou, C.-H. Chang, M.-H. Tsai and C.-C. Wu, *Angew. Chem., Int. Ed.*, 2007, **46**, 2418; (*f*) C. Ulbricht, B. Beyer, C. Friebe, A. Winter and U. S. Schubert, *Adv. Mater.*, 2009, **21**, 4418; (*g*) L. Flamigni, A. Barbieri, C. Sabatini, B. Ventura and F. Barigelletti, *Top. Curr. Chem.*, 2007, **281**, 143; (*h*) C.-M. Che, C.-C. Kwok, S.-W. Lai, A. F. Rausch, W. J. Finkenzeller, N. Zhu and H. Yersin, *Chem.–Eur. J.*, 2010, **16**, 233; (*i*) J. A. G. Williams, *Top. Curr. Chem.*, 2007, **281**, 205; (*j*) J. A. G. Williams, S. Develay, D. L. Rochester and L. Murphy, *Coord. Chem. Rev.*, 2008, **252**, 2596; (*k*) J. Kalinowski, V. Fattori, M. Cocchi and J. A. G. Williams, *Coord. Chem. Rev.*, 2011, **255**, 2401; (*l*) P.-T. Chou and Y. Chi, *Eur. J. Inorg. Chem.*, 2006, 3319; (*m*) J. Breu, C. Kratzer and H. Yersin, *J. Am. Chem. Soc.*, 2000, **122**, 2548.

4 (*a*) M. G. Crestani, G. F. Manbeck, W. W. Brennessel, T. M. McCormick and R. Eisenberg, *Inorg. Chem.*, 2011, **50**, 7172; (*b*) M. Hashimoto, S. Igawa, M. Yashima, I. Kawata, M. Hoshino and M. Osawa, *J. Am. Chem. Soc.*, 2011, **133**, 10348; (*c*) A. Barbieri, G. Accorsi and N. Armaroli, *Chem. Commun.*, 2008, **19**, 2185; (*d*) C.-W. Hsu, C.-C. Lin, M.-W. Chung, Y. Chi, G.-H. Lee, P.-T. Chou, C.-H. Chang and P.-Y. Chen, *J. Am. Chem. Soc.*, 2011, **133**, 12085; (*e*) R. Czerwieniec, J. Yu and H. Yersin, *Inorg. Chem.*, 2012, **51**, 1975; (*f*) H. Yersin, A. F. Rausch, R. Czerwieniec, T. Hofbeck and T. Fischer, *Coord. Chem. Rev.*, 2011, **255**, 2622; (*g*) R. Czerwieniec, T. Hofbeck, O. Crespo, A. M. Laguna, M. Concepcion-Gimeno and H. Yersin, *Inorg. Chem.*, 2010, **49**, 3764; (*h*) K. A. Barakat, T. R. Cundari and M. A. Omary, *J. Am. Chem. Soc.*, 2003, **125**, 14228; (*i*) S. Igawa, M. Hashimoto, I. Kawata, M. Hoshino and M. Osawa, *Inorg. Chem.*, 2012, **51**, 5805; (*j*) D. M. Zink, M. Bächle, T. Baumann, M. Nieger, M. Kühn, C. Wang, W. Klopper, U. Monkowius, T. Hofbeck, H. Yersin and S. Bräse, *Inorg. Chem.*, 2013, **52**, 2292; (*k*) D. M. Zink, T. Baumann, M. Nieger, E. C. Barnes, W. Klopper and S. Bräse, *Organometallics*, 2011, **30**, 3275; (*l*) L. Zhang, B. Li and Z. Su, *J. Phys. Chem. C*, 2009, **113**, 13968; (*m*) A. Tsuboyama, K. Kuge, M. Furugori, S. Okada, M. Hoshino and K. Ueno, *Inorg. Chem.*, 2007, **46**, 1992; (*n*) G. F. Manbeck, W. W. Brennessel and R. Eisenberg, *Inorg. Chem.*, 2011, **50**, 3431; (*o*) L. Bergmann, J. Friedrichs, M. Mydlack, T. Baumann, M. Nieger and S. Bräse, *Chem. Commun.*, 2013, **49**, 6501.

5 (*a*) D. R. McMillin, M. T. Buckner and B. T. Ahn, *Inorg. Chem.*, 1977, **16**, 943; (*b*) M. T. Buckner and D. R. McMillin, *J. Chem. Soc., Chem. Commun.*, 1978, 759; (*c*) M. W. Blaskie and D. R. McMillin, *Inorg. Chem.*, 1980, **19**, 3519; (*d*) D. R. McMillin, J. R. Kirchhoff and K. V. Goodwin, *Coord. Chem. Rev.*, 1985, **64**, 83; (*e*) D. R. Crane, J. DiBenedetto, C. E. A. Palmer, D. R. McMillin and P. C. Ford, *Inorg. Chem.*, 1988, **27**, 3698; (*f*) D. R. McMillin and K. M. McNett, *Chem. Rev.*, 1998, **98**, 1201; (*g*) A. Lavie-Cambot, M. Cantuel, Y. Leydet, G. Jonusauskas, D. M. Bassani and N. D. McClenaghan, *Coord. Chem. Rev.*, 2008, **252**, 2572.

6 N. Armaroli, G. Accorsi, F. Cardinali and A. Listorti, *Top. Curr. Chem.*, 2007, **280**, 69.

7 (*a*) L. X. Chen, G. Jennings, T. Liu, D. J. Gosztola, J. P. Hessler, D. V. Scaltrito and G. J. Meyer, *J. Am. Chem. Soc.*, 2002, **124**, 10861; (*b*) L. X. Chen, G. B. Shaw, I. Novozhilova, T. Liu, G. Jennings, K. Attenkofer, G. J. Meyer and P. Coppens, *J. Am. Chem. Soc.*, 2003, **125**, 7022; (*c*) R. M. Everly and D. R. McMillin, *Photochem. Photobiol.*, 1989, **50**, 711; (*d*) E. M. Stacy and D. R. McMillin, *Inorg. Chem.*, 1990, **29**, 393; (*e*) I. I. Vorontsov, T. Graber, A. Y. Kovalevsky, I. V. Novozhilova, M. Gembicky, Y.-S. Chen and P. Coppens, *J. Am. Chem. Soc.*, 2009, **131**, 6566; (*f*) A. K. I. Gushurst, D. R. McMillin, C. O. Dietrich-Buchecker and J. P. Sauvage, *Inorg. Chem.*, 1989, **28**, 4070; (*g*) M. T. Miller, P. K. Gantzel and T. B. Karpishin, *J. Am. Chem. Soc.*, 1999, **121**, 4292; (*h*) Q. Zhang, J. Ding, Y. Cheng, L. Wang, Z. Xie, X. Jing and F. Wang, *Adv. Funct. Mater.*, 2007, **17**, 2983; (*i*) D. Chantal, *Coord. Chem. Rev.*, 2015, **282–283**, 19.

8 (*a*) D. V. Scaltrito, D. W. Thompson, J. A. O'Callaghan and G. J. Meyer, *Coord. Chem. Rev.*, 2000, **208**, 243; (*b*) N. Armaroli, *Chem. Soc. Rev.*, 2001, **30**, 113.

9 (*a*) D. G. Cuttell, S. M. Kuang, P. E. Fanwick, D. R. McMillin and R. A. Walton, *J. Am. Chem. Soc.*, 2002, **124**, 6; (*b*) D. Volz, D. M. Zink, T. Bocksrocker, J. Friedrichs, M. Nieger, T. Baumann, U. Lemmer and S. Bräse, *Chem. Mater.*, 2013, **25**, 3414; (*c*) B. Carlson, G. D. Phelan, W. Kaminsky, L. Dalton, X. Jiang, S. Liu and A. K.-Y. Jen, *J. Am. Chem. Soc.*, 2002, **124**, 14162; (*d*) T. McCormick, W.-L. Jia and S. Wang, *Inorg. Chem.*, 2006, **45**, 147; (*e*) R. Czerwieniec, K. Kowalski and H. Yersin, *Dalton Trans.*, 2013, **42**, 9826; (*f*) H. Ohara, A. Kobayashia and M. Kato, *Dalton Trans.*, 2014, **43**, 17317; (*g*) D. M. Zink, D. Volz, T. Baumann, M. Mydlak, H. Flügge, J. Friedrichs, M. Nieger and S. Bräse, *Chem. Mater.*, 2013, **25**, 4471; (*h*) L. Qin, Q. Zhang, W. Sun, J. Wang, C. Lu, Y. Cheng and L. Wang, *Dalton Trans.*, 2009, 9388; (*i*) J. Min, Q. Zhang, W. Sun, Y. Cheng and L. Wang, *Dalton Trans.*, 2011, **40**, 686; (*j*) Q. Zang, Q. Zhou, Y. Cheng, L. Wang, D. Ma, X. Jing and F. Wang, *Adv. Mater.*, 2004, **16**, 432; (*k*) Q. Zhang, Q. Zhou, Y. Cheng, L. Wang, D. Ma, X. Jing and F. Wang, *Adv. Funct. Mater.*, 2006, **16**, 1203; (*l*) N. Armaroli, G. Accorsi, M. Holler, O. Moudam, J.-F. Nierengarten, Z. Zhou, R. T. Wegh and R. Welter, *Adv.*

Mater., 2006, **18**, 1313; (*m*) G. Che, Z. Su, W. Li, B. Chu and M. Li, *Appl. Phys. Lett.*, 2006, **89**, 103511; (*n*) J.-L. Chen, X.-F. Cao, W. Gu, H.-R. Wen, L.-X. Shi, G. Rong and P. Luo, *Inorg. Chem. Commun.*, 2011, **14**, 1894.

10 C. A. Tolman, *Chem. Rev.*, 1977, **77**, 313.

11 (*a*) O. Maury and H. le Bozec, *Metal-based quadratic nonlinear optical materials*, John Wiley & Sons, UK, 2010, vol. 1, pp. 32–35; (*b*) O. Maury and H. le Bozec, *Acc. Chem. Res.*, 2005, **38**, 691; (*c*) C. E. Housecroft and E. C. Constable, *Chem. Soc. Rev.*, 2015, **44**, 8386; (*d*) M. Freitag, Q. Daniel, M. Pazoki, K. Sveinbjörnsson, J. Zhang, L. Sun, A. Hagfeldt and G. Boschloo, *Energy Environ. Sci.*, 2015, **8**, 2634.

12 P. C. Ford, E. Cariati and J. Bourassa, *Chem. Rev.*, 1999, **99**, 3625.

13 D. J. Eisler, C. W. Kirby and R. J. Puddephatt, *Inorg. Chem.*, 2003, **42**, 7626.

14 (*a*) R. Czerwieniec, J. Yu and H. Yersin, *Inorg. Chem.*, 2011, **50**, 8293; (*b*) U. Monkowius, S. Ritter, B. König, M. Zabel and H. Yersin, *Eur. J. Inorg. Chem.*, 2007, 4597; (*c*) S.-H. Kuang, D. G. Cuttell, D. R. McMillin, P. E. Fanwick and R. A. Walton, *Inorg. Chem.*, 2002, **41**, 3313.

15 R. Caris, B. C. Peoples, M. Valderrama, G. Wu and R. Rojas, *J. Organomet. Chem.*, 2009, **694**, 1795.

16 M. Kranenburg, Y. E. M. van der Burgt, P. C. J. Kamer and P. W. N. M. van Leeuwen, *Organometallics*, 1995, **14**, 3081.

17 M. A. Escobar, D. H. Jara, R. A. Tapia, L. Lemus, R. Fröhlich, J. Guerrero and R. S. Rojas, *Polyhedron*, 2013, **62**, 66.

18 G. Accorsi, A. Listorti, K. Yoosaf and N. Armaroli, *Chem. Soc. Rev.*, 2009, **38**, 1690.

19 G. Scalmani and M. J. Frisch, *J. Chem. Phys.*, 2010, **132**, 114110.

20 C. Femoni, S. Muzzioli, A. Palazzi, S. Stagni, S. Zacchini, F. Monti, G. Accorsi, M. Bolognesi, N. Armaroli, M. Massi, G. Valenti and M. Marcaccio, *Dalton Trans.*, 2013, **42**, 997.

21 J. Bard and L. R. Faulkner, *Electrochemical methods: fundamentals and applications*, Wiley, New York, 2nd edn, 2001.

22 (*a*) L. He, L. Duan, J. Qiao, R. Wang, P. Wei, L. Wang and Y. Qiu, *Adv. Funct. Mater.*, 2008, **18**, 2123; (*b*) R. D. Costa, E. Orti, H. J. Bolink, F. Monti, G. Accorsi and N. Armaroli, *Angew. Chem., Int. Ed.*, 2012, **51**, 8178.

23 F. Lafolet, S. Welter, Z. Popovic and L. de Cola, *J. Mater. Chem.*, 2005, **15**, 2820.

24 M. W. Mara, K. A. Fransted and L. X. Chen, *Coord. Chem. Rev.*, 2015, **282–283**, 2.

25 A. D. Becke, *J. Chem. Phys.*, 1993, **98**, 5648.

26 P. J. Hayand and W. R. Wadt, *J. Chem. Phys.*, 1985, **82**, 299.

27 M. Cossi, V. Barone, B. Mennucci and J. Tomasi, *Chem. Phys. Lett.*, 1998, **286**, 253.

28 T. Lu and F. Chen, *J. Comput. Chem.*, 2012, **33**, 580.